

# Synthesis, Characterization, Optical Properties, and Electron Paramagnetic Resonance for Nano $\text{Zn}_{0.5}\text{Co}_{0.5}\text{Fe}_{2-x}\text{Pr}_x\text{O}_4$

Z. Bitar<sup>1</sup> · S. Isber<sup>2</sup> · S. Nouredine<sup>3</sup> · D. El-Said Bakeer<sup>4</sup> · R. Awad<sup>1</sup>

Received: 20 May 2016 / Accepted: 27 October 2016 / Published online: 15 November 2016  
© Springer Science+Business Media New York 2016

**Abstract** Nano ferrite samples of type  $\text{Zn}_{0.5}\text{Co}_{0.5}\text{Fe}_{2-x}\text{Pr}_x\text{O}_4$ ,  $0 \leq x \leq 0.2$ , were prepared by co-precipitation method for different concentration of Pr ions at a calcination temperature of 823 K. The samples were characterized using x-ray diffraction and transmission electron microscope (TEM), UV spectroscopy, FTIR, and electron paramagnetic resonance (EPR). The increase in concentration of Pr ions shows a significant change in the formed nano ferrite particles size, degree of aggregation, energy band gap, and lattice parameters. X-band (9.24 GHz) EPR spectra at room temperature showed a decrease in the  $g$  factor as the Pr content was increased. Furthermore, the variation of the  $\text{Pr}^{3+}$  concentration in the samples led to different aggregation states, ranging from isolated nanoparticles with average crystal size of 28.5 to about 15 nm, as confirmed by x-ray diffraction and high-resolution transmission electron microscopy.

**Keywords** Nanoferrite ·  $\text{CoZnFe}_2\text{O}_4$  ·  $\text{Co}_{0.5}\text{Zn}_{0.5}\text{Fe}_{2-x}\text{Pr}_x\text{O}_4$  · XRD · TEM · EPR

## 1 Introduction

In recent years, ferrites and ferrite-based compounds have been attracting much attention due to their potential application in magnetic recording media, magnetic fluids, catalysis agents, gas sensors, and biomedical equipment [1–6].

The first systematic study on the relationship between chemical composition and magnetic properties of various ferrites was reported by Hilpert in 1909. Hilpert had successfully prepared spinel ferrites, such as manganese, copper, cobalt, magnesium, and zinc. Later on, in 1960, Feynman revisited this particular idea in his article “there is plenty of room at the bottom” [7] where he discussed his thoughts for creating innovative low-dimensional materials at the *nanoscale*. In the last two decades, material scientists paid increasing attention to the implications of size effects on material properties and the field of *nanotechnology* attained a leading role. Meanwhile, research on nanosized materials has developed into a large interdisciplinary field of research which opened the era of material science. The most important feature of these nanomaterials is given by their chemical and physical properties which markedly differ from those of the *bulk* [8].

The preparation of nano ferrites can be done by various physical and chemical methods like sol-gel, ball milling, chemical combustion, co-precipitation, etc. In the present work, we chose the co-precipitation method because of its simplicity and its suitability for better control of the particle sizes and shapes [9].

Spinel ferrites, which are formed by a nearly close-packed fcc array of anions with holes partly filled by the cations, can be represented by the formula  $(M_{1-\delta}\text{Fe}_\delta)_A(M_\delta\text{Fe}_{2-\delta})_B\text{O}_4$ , where  $A$  and  $B$  represent the tetrahedral and octahedral sites, respectively.  $M$  represents

✉ S. Isber  
samih.isber@aub.edu.lb

<sup>1</sup> Physics Department, Beirut Arab University, Beirut, Lebanon

<sup>2</sup> Physics Department, American University of Beirut, Bliss Street, 11-0236, Beirut, Lebanon

<sup>3</sup> Physics Department, Lebanese University, Beirut, Lebanon

<sup>4</sup> Physics Department, Damanhur University, Damanhour, Egypt

divalent ions like Mn, Co, Ni, Zn, or Mg and  $\delta$  represents the inversion parameter [10]. The structural and magnetic properties of spinel ferrite depend on the distribution of cations over the two sub lattices, tetrahedral *A* sites and octahedral *B* sites which are occupied by different metal ions.  $\text{Co}_{0.5}\text{Zn}_{0.5}\text{Fe}_2\text{O}_4$  is a mixed spinel with Zn and Co ions occupying the tetrahedral *A* sites and the octahedral *B* sites, respectively [11].

Rare earth ions with unpaired 4f electrons have strong spin-orbit coupling of angular momentum. The introduction of rare earth ions into spinel ferrites would result in a 4f-3d coupling through the  $\text{RE}^{3+}\text{-Fe}^{3+}$  interactions which will determine the magneto crystalline anisotropy of the material. Doping with rare earth ions is also helpful in reducing the grain size of the materials and it affects the lattice parameters. Indeed, substituting  $\text{Fe}^{3+}$  by a larger-sized rare earth ion would normally increase the lattice parameters and reduce some of the strain in the lattice. Shahane et al. investigated the effect of Zn substitution on the structural and magnetic properties of Ni–Co ferrites. They reported a linear increase of the lattice parameter with increasing Zn content. They have also used Neel's collinear two-sub-lattice model to explain the behavior of the magnetization saturation as function of Zn content [12]. Moreover, Kuar et al. studied the effect of  $\text{Gd}^{3+}$  ions substituted in  $\text{Ni}_{0.5}\text{Zn}_{0.5}\text{Gd}_x\text{Fe}_{2-x}\text{O}_4$  ferrite nanoparticles by electron paramagnetic resonance (EPR). A decrease in the Landé value and an increase in relaxation time was found. These results were correlated with the change of particle size as function of  $\text{Gd}^{3+}$  concentrations [13]. Ahamed et al. investigated the effect of introducing rare earth cations into the ferrites spinel structure of type  $\text{MgCe}_x\text{Er}_y\text{Fe}_{2-x-y}\text{O}_4$ . They found out that these materials can be suitable for Microstrip patch antenna since they increase the gain and improve the directivity of antenna [14]. Sahib et al. also succeeded in growing  $\text{ZnNi}_y\text{Ce}_x\text{Fe}_{2-x-y}\text{O}_4$  [15] and measured the saturation magnetization versus Ce content. They have also investigated the semiconducting behavior of their compounds.

In the work, we present the effect of  $\text{Pr}^{3+}$  content on the structural, optical, and magnetic properties of Co-Zn ferrite. The variation of various  $\text{Pr}^{3+}$  doping level on these properties are also discussed.

## 2 Experimental

Nanosized ( $\text{Co}_{0.5}\text{Zn}_{0.5}\text{Fe}_{2-x}\text{Pr}_x\text{O}_4$ ),  $0.0 \leq x \leq 0.3$  were prepared by Co precipitation method. The analytical grade chemical reagents are iron (III) chloride hexahydrate ( $\text{FeCl}_3 \bullet 6\text{H}_2\text{O}$ ), cobalt (II) chloride hydrate ( $\text{CoCl}_2 \bullet x\text{H}_2\text{O}$ ), zinc chloride ( $\text{ZnCl}_2$ ), and praseodymium (III) chloride ( $\text{PrCl}_3 \bullet x\text{H}_2\text{O}$ ) were taken in stoichiometric amounts of

ratios. The nano ferrites were then dissolved in distilled water and mixed using magnetic stirrer at 40 ° C. For coprecipitation of such prepared solution, a solution of NaOH (4 M) was added in drop-wise with constant stirring produced by a magnetic stirrer. The pH of the solution was maintained at 12.5–13 in order to transform the hydroxides of metals into nano particles. The solution was maintained at 60 ° C with constant stirring for 2 h. This duration was sufficient for the transformation of hydroxides into spinel ferrite. The precipitated particles were then washed several times with distilled water to remove the impurities. The precipitated particles were then dried in an oven at 97 ° C for 24 h. The resulting solid was grinded into powder and calcined at temperature 823 K for 6 h.

The nanosized ( $\text{Co}_{0.5}\text{Zn}_{0.5}\text{Fe}_{2-x}\text{Pr}_x\text{O}_4$ ) were characterized by XRD using Bruker D8 advance powder diffractometer with Cu–K $\alpha$  radiation ( $\lambda = 1.54056 \text{ \AA}$ ) in the range  $10^\circ \leq 2\theta \leq 80^\circ$ . In order to examine the morphology of the nanoparticles, we used Jeol transmission electron microscope (TEM) JEM-100CX, operated at 80 kV. For the TEM measurements, the samples were prepared by placing small drop of nanoparticle dispersion liquid on a copper grid and dried with air at room temperature for several hours.

The FTIR measurements were carried out using an FTIR 8400S Shimadzu UV-visible spectrometer. The absorption spectra of the samples have been taken in the wavelength range from 200 to 600 nm by using Jasco-V-670 - UV-Visible spectrometer.

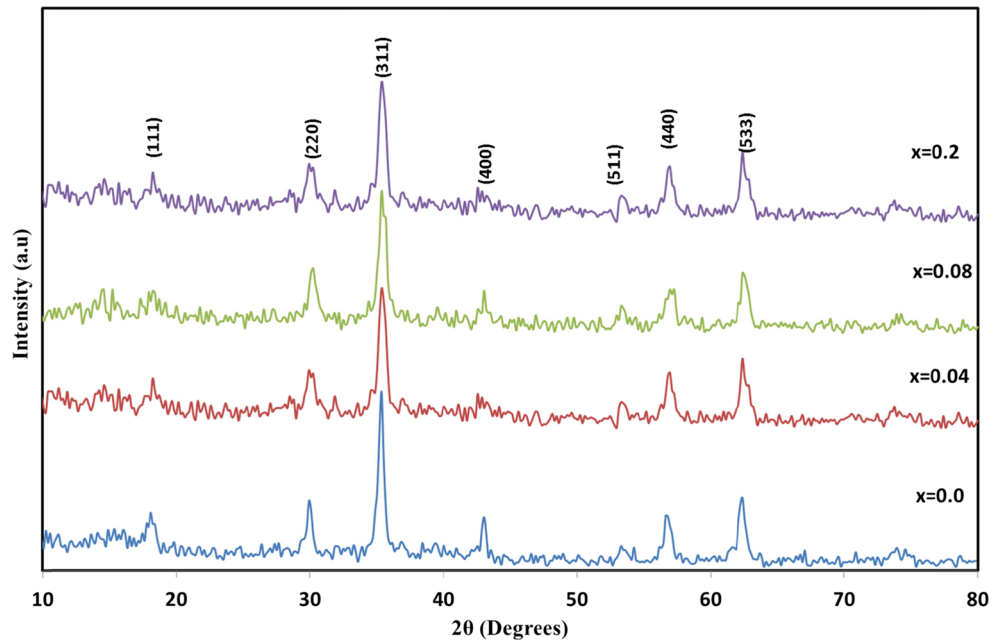
EPR spectra of samples with various  $\text{Pr}^{3+}$  content were investigated using a Bruker X-band (9.24 GHz), a systematic study on the *g* values and peak to peak line width  $\Delta H_{pp}$  was made. In order to obtain a broad and sharp signal the receiver gain was placed at 10 mV, microwave power at ~12 mw, and field modulation amplitude ~20 G at 100 KHz.

## 3 Results and Discussion

### 3.1 X-Ray Diffraction Studies

XRD spectra of  $\text{Co}_{0.5}\text{Zn}_{0.5}\text{Fe}_{2-x}\text{Pr}_x\text{O}_4$ ,  $0.00 \leq x \leq 0.2$ , are shown in Fig. 1. All the characteristic diffraction peaks correspond to the cubic spinel structure of  $\text{Co}_{0.5}\text{Zn}_{0.5}\text{Fe}_2\text{O}_4$  (JCPDS Card no. 22-1086) [16, 17] with space group Fd3m. The peaks in the XRD pattern of the samples can be perfectly indexed to the (111), (220), (311), (400), (422), (511), (440), and (533) facets of the  $\text{Co}_{0.5}\text{Zn}_{0.5}\text{Fe}_2\text{O}_4$  phase (as shown in Fig. 1). The diffraction peaks are broad because of the nanometer size of the crystallites. It is worthwhile mentioning that no additional or impurity phases corresponding to any other structure were detected in the XRD spectra which confirms that  $\text{Pr}^{3+}$  ions have been incorporated into spinel lattice. The main peak corresponding

**Fig. 1** XRD spectra of  $Zn_{0.5}Co_{0.5}Fe_{2-x}Pr_xO_4$  for various  $Pr^{3+}$  concentrations



to the crystal plane with Miller indices of (311) was centered between  $2\theta = 35.28^\circ$  and  $35.65^\circ$ , for all samples  $Co_{0.5}Zn_{0.5}Fe_{2-x}Pr_xO_4$  with  $0 \leq x \leq 0.2$ ; this confirms the presence of cubic face structure of  $Co_{0.5}Zn_{0.5}Fe_{2-x}Pr_xO_4$  nanoparticles.

The average crystallite size is calculated using Dbye-Scherrer’s equation:

$$D = \frac{0.9\lambda}{\beta \cos\theta} \tag{1}$$

where  $\theta$  is the diffraction angle,  $\lambda$  is the wavelength of incident x-ray and  $\beta$  is the full width at half maximum (FWHM) of the XRD peak in units of radians [18, 19]. The estimated values of the crystallite sizes are given in Table 1. It was found that the crystallites sizes decrease with increasing the concentration of  $Pr^{3+}$  ions in the samples. This may be due to the larger ionic radius of  $Pr^{3+}$  ions ( $0.99 \text{ \AA}$ ) as compared to that of  $Fe^{3+}$  ions ( $0.645 \text{ \AA}$ ) which required more energy to make  $Pr^{3+}$  ions enter into the *B* sites to complete crystallization and grains formation [20]. The average crystallites’ size value of undoped  $Co_{0.5}Zn_{0.5}Fe_2O_4$  was

found to be larger than that reported for similar samples prepared by co-precipitation method for which the nanosized powder were annealed at 573 K for 24 h [21].

The lattice constant *a* of our samples (spinel structure) was calculated from the position of the prominent peak (311) using Bragg’s equation:

$$a = d_{hkl} \sqrt{h^2 + k^2 + l^2} \tag{2}$$

where *a* is the lattice parameter;  $d_{hkl}$  is the lattice spacing; and *h*, *k* and *l* are the miller indices. It was found that the lattice constant decreases with increasing  $Pr^{3+}$  concentration ions (as shown in Table 1). This can be attributed to the large ionic radius of ion which prevents it from occupying the tetrahedral and the octahedral sites which form aggregates on the grain boundary [22]. As  $Pr^{3+}$  ion content increases, the aggregates increases and lead to further compression in the spinel lattice. The lattice parameter value obtained for pure  $Co_{0.5}Zn_{0.5}Fe_2O_4$  is in good agreement with the reported value [16].

**Table 1** Crystallite size using Sherrer equation (max peak) and TEM, lattice parameter *a* the values of  $\nu_1$ ,  $\nu_2$ , and energy gap for different concentration of  $Pr^{3+}$  ( $0.00 \leq x \leq 0.20$ )

Pr content	XRD		TEM	FTIR		UV
	<i>D</i> (nm)	Lattice constant ( <i>a</i> ) (Å)	<i>D</i> (nm)	$\nu_1$ (cm <sup>-1</sup> )	$\nu_2$ (cm <sup>-1</sup> )	Band energy (eV)
0	28.3	8.4404	7.74	570.95	434.00	3.06
0.04	19.4	8.4349	7.39	576.74	449.43	3.08
0.08	18.7	8.4291	7.25	586.38	430.14	3.09
0.2	14.7	8.4057	6.30	632.67	441.71	3.12

### 3.2 TEM Studies

The TEM images of nanosized  $\text{Co}_{0.5}\text{Zn}_{0.5}\text{Fe}_{2-x}\text{Pr}_x\text{O}_4$ ,  $x = 0.0, 0.04, 0.08$ , and  $0.2$  are shown in Fig. 2. The images show that the particles are spherical in shape with the presence of some moderately agglomerated particles as well as isolated particles. It was also observed that the average grain size is decreased with increasing  $\text{Pr}^{3+}$  concentration as per their values listed in Table 1. This decrease in grain size was also obtained from the analysis of the XRD measurements. We observed that the particle sizes estimated from TEM images are rather smaller than those estimated from Scherrer's equation using the XRD spectra. This difference is probably due to the fact that the samples for TEM measurements were prepared from reaction solution and not from powder. At this point, aging conditions play a decisive role in the particles sizes. Particle sizes in reaction solution are susceptible to aging effects which in turn may result in high band gap energy. Thus, we believe that aging in reaction solution is one of the main effects responsible for deviation in sizes measured by XRD and TEM.

### 3.3 FTIR Studies

In addition to the XRD characterization, we ran a series of FTIR spectra on our samples to further investigate their

purities and their structural compositions. The FTIR spectra of the prepared samples with different concentrations of  $\text{Pr}^{3+}$  ions are shown in Fig. 3. They confirm the formation of spinel structure by the presence of the two main absorption bands with very low intensities in the range  $700\text{--}400\text{ cm}^{-1}$ . The highest absorption band,  $\nu_1$ , was observed in the range  $700\text{--}500\text{ cm}^{-1}$ ; it corresponds to intrinsic stretching vibrations of the metal at the tetrahedral site,  $M_{\text{tetra}} \longleftrightarrow \text{O}$ . The lowest band,  $\nu_2$ , was observed in the range  $500\text{--}400\text{ cm}^{-1}$ , and it corresponds to octahedral metal stretching,  $M_{\text{octa}} \longleftrightarrow \text{O}$  (see Table 1). The observed shift in the bands of the doped samples can be attributable to a difference in the metal ion–oxygen distance for the two sublattices [23] and the change in the lattice constant [24]. The slight shift in the  $\nu_1$  bands with increasing the concentration of  $\text{Pr}^{3+}$  ions can be contributing to the variation of the metal–oxygen bonds in the tetrahedral sites due to the transition between the extent of normal spinel and inverse structures. The shift of  $\nu_2$  as a function of Pr content shows an increase followed by a decrease at higher Pr content which may be due to mixed cationic distribution at the tetrahedral sites [25–27]. The broad band ( $3600\text{--}3200\text{ cm}^{-1}$ ) centered at  $3423.76\text{ cm}^{-1}$  can be assigned to hydrogen-bonded O–H stretching vibration arising from absorbed water which shows the presence of humidity in the prepared samples.

**Fig. 2** TEM images for nano  $\text{Zn}_{0.5}\text{Co}_{0.5}\text{Fe}_{2-x}\text{Pr}_x\text{O}_4$ . **a**  $x = 0.00$ , **b**  $x = 0.04$ , **c**  $x = 0.08$ , and **d**  $x = 0.2$

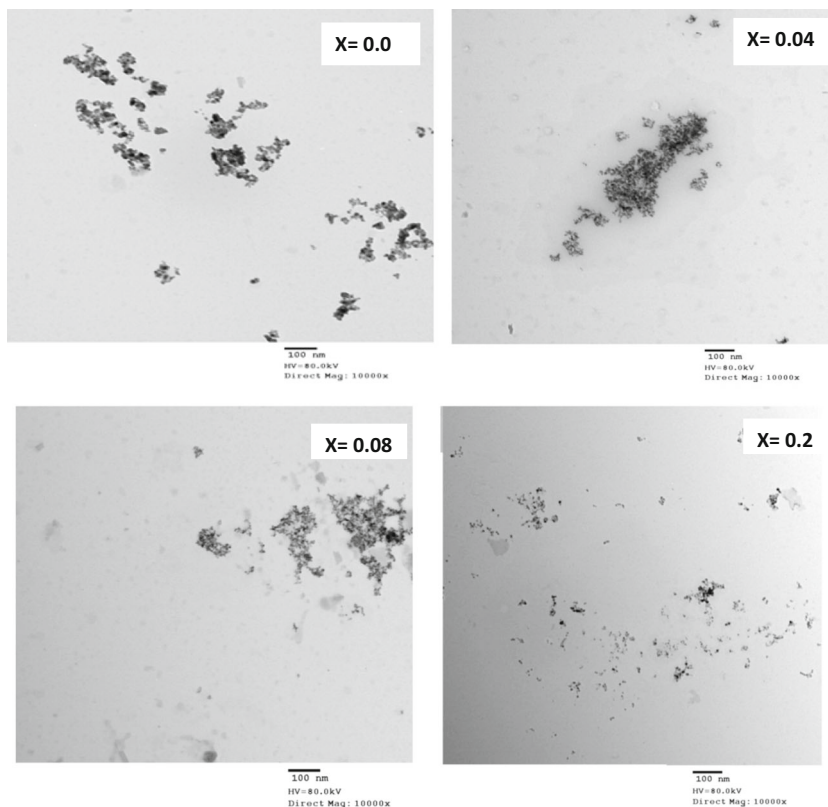
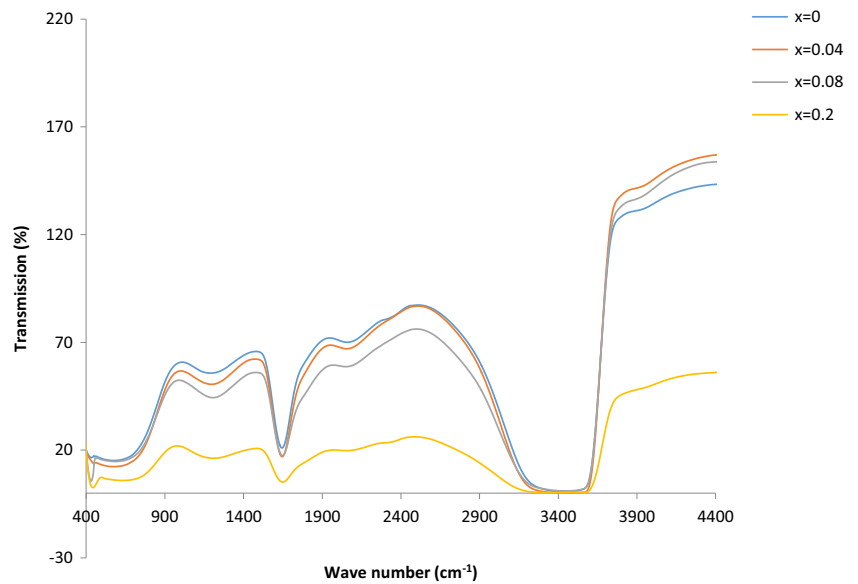


**Fig. 3** FTIR spectra of the samples for  $x = 0, 0.04, 0.08,$  and  $0.2$



### 3.4 UV-VIS Spectroscopy

Many models were used to determine the optical properties of nano ferrites. In the present study, we used

the Tauc model. The optical gap associated with the  $\text{Co}_{0.5}\text{Zn}_{0.5}\text{Fe}_{2-x}\text{Pr}_x\text{O}_4$  nano ferrites was determined by plotting  $(\alpha h\nu)^2$  over a limited range of photon energies  $h\nu$  and extrapolation the linear part of the curve  $(\alpha h\nu)^2 = 0,$

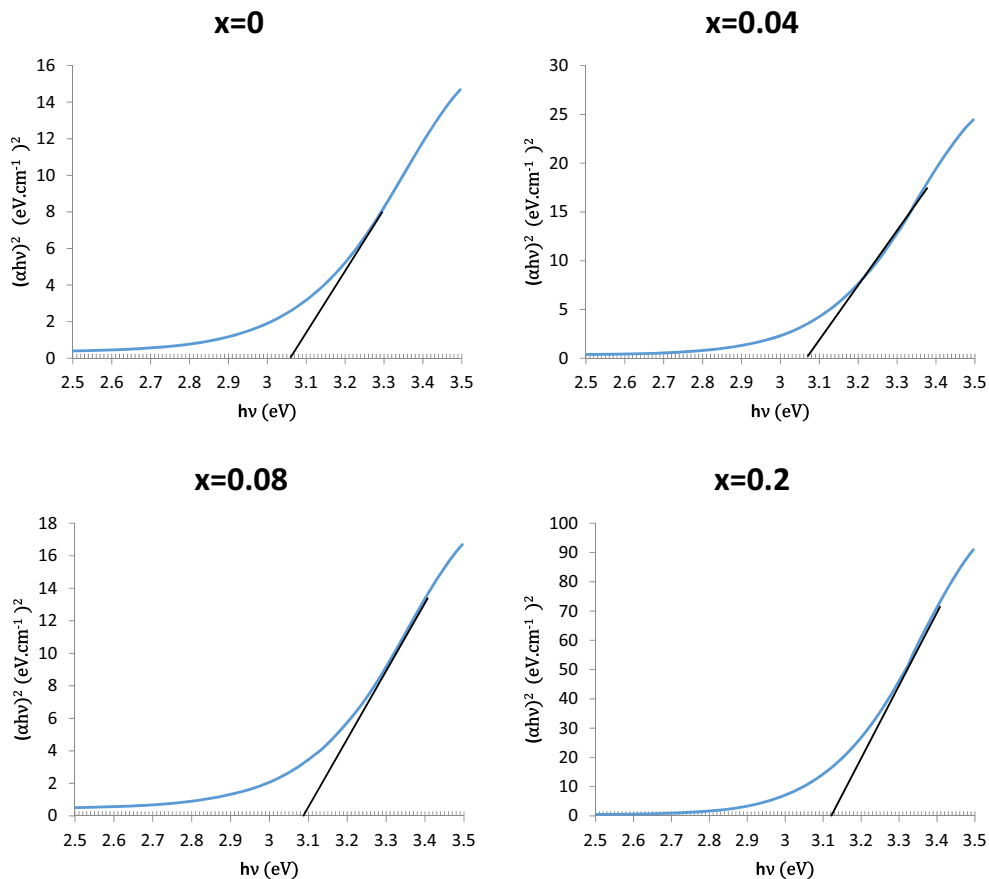


**Fig. 4** Photoresponse versus energy curves for the determination of the optical band gap energy for  $\text{Zn}_{0.5}\text{Co}_{0.5}\text{Fe}_{2-x}\text{Pr}_x\text{O}_4$  ( $0 \leq x \leq 0.2$ )



as shown in Fig. 4. The absorption coefficient ( $\alpha$ ) was calculated using the measured absorbance ( $A$ )

$$\alpha = 2.303 \frac{A}{t}, \quad (3)$$

where  $t$  is the thickness of the sample.

Tauc optical gap is defined as occurring at the intercept of this linear extrapolation with  $Y$ -axis. The absorption coefficient  $\alpha$  near the band edge in many nano ferrites shows an exponential behavior upon the photon energy that may be described by:

$$(\alpha h\nu)^n = A(h\nu - E_g) \quad (4)$$

where  $E_g$  is the energy band gap energy,  $n$  is either 2 for a direct band gap material or  $\frac{1}{2}$  for indirect band gap material, and  $(h\nu)$  is incident photon energy. The energy band gap listed in Table 1 were calculated for  $n = 2$  [28]. The obtained values (Table 1) of the optical band gap show an increase with increasing the concentration of  $\text{Pr}^{3+}$  ions, which is in conformity with the decrease of the particle size as obtained by TEM and x-ray measurements.

### 3.5 EPR Measurements

X-Band EPR spectra (9.24 GHz) were recorded at room temperature for  $\text{Co}_{0.5}\text{Zn}_{0.5}\text{Fe}_{2-x}\text{Pr}_x\text{O}_4$  with various  $\text{Pr}^{3+}$  concentrations are shown in Fig. 5. A single, strong and broad symmetric EPR signal was observed for all samples with the resonance magnetic field  $H_r$  shifting to higher values as the  $\text{Pr}^{3+}$  content was increased.

The spectroscopic Landé factor ( $g$  value) was determined from the magnetic resonance field  $H_r$  by:

$$g = \frac{h\nu}{\beta H_r} \quad (5)$$

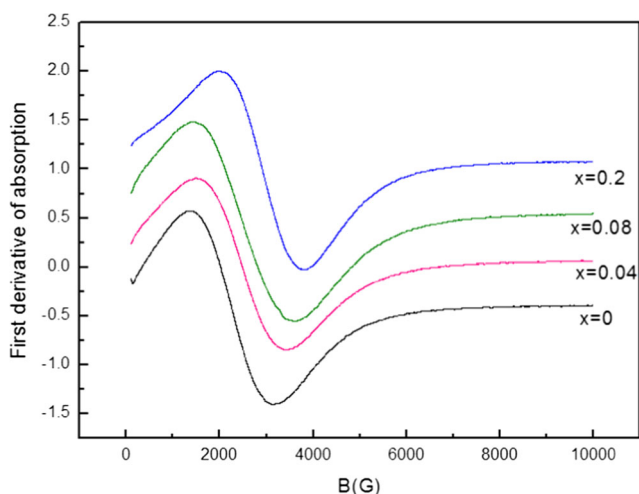


**Fig. 5** Room temperature EPR spectra (9.25 GHz) for  $\text{Zn}_{0.5}\text{Co}_{0.5}\text{Fe}_{2-x}\text{Pr}_x\text{O}_4$  ( $0 \leq x \leq 0.2$ )

**Table 2** Variation of  $g$  value, resonance field ( $H_r$ ), peak to peak line width ( $\Delta H_{pp}$ ) for nano  $\text{Zn}_{0.5}\text{Co}_{0.5}\text{Fe}_{2-x}\text{Pr}_x\text{O}_4$

Pr content	$H_r$ (gauss)	$g$ value	$\Delta H_{pp}$ (gauss)
$x = 0$	2132	3.097	2016
$x = 0.04$	2435	2.712	2701
$x = 0.08$	2405	2.746	2473
$x = 0.2$	2826	2.337	2172

where  $h$  is Planck's constant,  $\nu$  is the microwave frequency (9.24 GHz),  $\beta$  is the Bohr magneton. All the spectra were analyzed and fitted to a single EPR absorption line to obtain the values of magnetic resonance fields  $H_r$ ,  $g$  values and peak to peak ( $\Delta H_{pp}$ ) line width. The calculated values are listed in Table 2.

The EPR spectra show that as the  $\text{Pr}^{3+}$  content was increased, the EPR lines were broadened and shifted to higher resonance fields. This behaviour could be explained by a strong dipolar interaction and decrease in super exchange interactions which lead to the broadening of the resonance line. The  $g$ -values were found to decrease from  $3.10 \pm 0.01$  to  $2.34 \pm 0.01$  with increasing  $\text{Pr}^{3+}$  ion concentration. The decrease in the  $g$  values may be attributed to a super exchange interaction between  $\text{Fe}^{2+}$  and  $\text{Fe}^{3+}$  at octahedral  $B$  sites [29]. As the concentration of  $\text{Pr}^{3+}$  is increased, the peak-to-peak line width ( $\Delta H_{pp}$ ) increases to reach maximum values for samples with  $x = 0.08$ . However, when the concentration of  $\text{Pr}^{3+}$  ions becomes sufficiently high the extra process of exchange narrowing comes to be effective. The decrease in the EPR line width at high concentrations could be due to the Anderson exchange narrowing [30]. The exchange narrowing is a mark of clustering of magnetic ions in samples with high  $\text{Pr}^{3+}$  contents.

### 4 Conclusions

Zn–Co nano ferrite doped with Pr ions ( $\text{Zn}_{0.5}\text{Co}_{0.5}\text{Fe}_{2-x}\text{Pr}_x\text{O}_4$ ) has been successfully synthesized using co-precipitation method. The x-ray diffraction confirmed the formation of single-phase cubical spinel structure with size in the range 14.7–28.3 nm. The XRD profiles showed a decrease in the lattice constant and crystallite size with the increase in the concentration of  $\text{Pr}^{3+}$  ions. TEM results showed the distribution of grains and morphology of the samples. The formation of the ferrite nanoparticles was confirmed from the metal–oxygen (M–O) vibration bands of the FTIR spectra. A slight shift in the bands of the substituted samples was observed due to the change in the lattice constant. The band gaps calculated from the UV–Vis spectroscopy show an increase from 3.05 to 3.12 eV with the increase of  $\text{Pr}^{3+}$  ions concentration. EPR studies show

dependence of EPR parameters on  $\text{Pr}^{3+}$  concentrations. The  $g$  factor decreases from 3.097 to 2.337, the resonance magnetic field increases from 2132 to 2826 gauss. The decrease in  $g$  value is associated with increase in particle size as  $\text{Pr}^{3+}$  ions concentration increases in Zn–Co nano ferrite. Also, the increase in  $\text{Pr}^{3+}$  concentrations increased the dipolar interaction and decreased the super exchange interactions.

**Acknowledgments** This work was performed in the Materials Science Lab, Physics Department, Beirut Arab University, Beirut, Lebanon, and at the Physics Department of the American University of Beirut, Lebanon.

## References

- Schmidtmeier, D., Buchel, G., Buhr, A.: *Mater. Ceram.* **61**, 223–227 (2009)
- Hulbert, D.M., Jiang, D., Kuntz, J.D., Kodera, Y., Mukherjee, A.K.: *Scr. Mater.* **56**, 1103–1106 (2007)
- Tsoncheva, T., Manova, E., Velinov, N., Paneva, D., Popova, M., Kunev, B., Tenchev, K., Mitov: *I. Catal. Commun.* **12**, 105–109 (2010)
- Kang, K.S., Kim, C.H., Cho, W.C., Bae, K.K., Woo, S.W., Park, C.S.: *Int. J. Hydrog. Energy* **33**, 4560–4568 (2008)
- Nasrallah, N., Kebir, M., Koudri, Z., Trari, M.: *J. Hazard. Mater.* **185**, 1398–1404 (2011)
- Kameoka, S., Tanabe, T., Tsai, A.P.: *Appl. Catal. A: Gen.* **375**, 163–171 (2010)
- Stylios, G.K., Feynman, R.P.: *Int. J. Cloth. Sci. Tech.* **25**, 336–347 (2013)
- Erdem, E.: *Hybrid Mater.* **1**, 62–70 (2014)
- Amarjeet, Kumar, V.: *Inter. J. Lat. Res. Sc. Tech.* **3**, 61–63 (2014)
- Kim, C.S., Lee, S.W., Park, S.L., Park, J.Y., Park, Y.J.: *J. Appl. Phys.* **79**, 5428 (1996)
- Petitt, G.A., Forester, D.W.: *Phys. Rev. B* **4**, 3912 (1971)
- Shahane, G.S., Kumar, A., Arora, M., Pant, R.P., Krishan, L.: *J. Magn. Magn. Mater.* **322**, 1015–1019 (2010)
- Kaur, B., Arora, M., Shankar, A., Kumar, A.S., Rajendra, P.P.: *Adv. Mat. Lett.* **3**(4), 399–405 (2012)
- Ahamed, S.K., Sahib, A.K., Suganthi, M., Naidu, V., Pandian, S., Sivabharathy, M.: *Int. J. Chem. Tech. Res.* **6**, 4615–4624 (2014)
- Sahib, A.K., Suganthi, M., Naidu, V., Pandian, S., Sivabharathy, M.: *Int. J. Chem. Tech. Res.* **6**, 4165 (2014)
- Praveena, K., Sadhana, K.: *Int. J. Sci. Res. Publ.* **5**, 2250–3153 (2015)
- Vaidyanathan, G., Sendhlnathan, S., Arulmurugan, R.: *J. Magn. Magn. Mater.* **313**, 293 (2007)
- Vinuthna1, C.H., Ravinder, D., Madhusudan, R., Ravinder, D., et al.: *Int. J. Eng. Res. Appl.* **3**, 2248–9622 (2013)
- Kumar, R., Singh, R.R., Barman, P.B.: *Int. J. Sci. Eng. Res.* **5**, 2229–5518 (2014)
- Meng, Y.Y., Liu, Z.W., Dai, H.C., Yu, H.Y., Zeng, D.C., Shukla, S., Ramanujan, R.V.: *Powder. Tech.* **229**, 270–275 (2012)
- Sudheesh, V.D., Bhargava, H., Suwalka, O., Lakshmi, N., Reddy, V.R., Venugopalan, K., Gupta, A.: *Hyperfine Interact.* **199**, 403 (2011)
- Ateia, E.E., Ahmed, M.A., Salah, L.M., El-Gamal, A.A.: *Phys. B* **445**, 60 (2014)
- Labade, B.K., Sable, M.C., Shamkwar, N.R.: *Mater. Lett.* **57**, 1651 (2003)
- Patange, S.M., Shirsath, S.E., Lohar, K.S., Algude, S.G., Kamble, S.R., Kulkarni, N., Mane, D., Jadhav, K.M.: *J. Magn. Magn. Mater.* **325**, 107 (2013)
- Balakrishnan, P., Veluchamy, P.: *Int. J. ChemTech Res.* **8**, 271–276 (2015)
- Xavier, S., Thankachan, S., Jacob, B.P., Mohammed, E.M.: *Nanosystems: Phys. Chem. Math.* **4**, 430–437 (2013)
- Praveena, K., Sadhana, K.: *Int. J. Sci. Res. Publ.* **5**, 2250–3153 (2015)
- Thakur, P., Sharma, R., Sharma, V., Sharma, P.: *Natl. Conf. Recent Innov. Appl. Sci. Humanit.* **4**, 2277–8179 (2015)
- Venkataram, C., Paulsingh, R.: *Int. J. Nano Dimens. Nat. Conf. Recent Innov. Appl. Sci. Humanit.* **4**, 183 (2015)
- Anderson, P.W., Weiss, P.R.: *Rev. Mod. Phys.* **25**, 269 (1953)